

Ferroelectric Soft Phonons, Charge Density Wave Instability and Strong Electron-Phonon Coupling in BiS₂-Layered Superconductors

T. Yildirim^{1,2,*}

¹*NIST Center for Neutron Research, National Institute of Standards and Technology, Gaithersburg, Maryland 20899, USA*

²*Department of Materials Science and Engineering,
University of Pennsylvania, Philadelphia, PA 19104, USA*

(Dated: November 5, 2018)

Very recently a new family of layered materials, containing BiS₂ planes was discovered to be superconducting at temperatures up to T_c=10 K, raising questions about the mechanism of superconductivity in these systems. Here, we present state-of-the-art first principles calculations that directly address this question and reveal several surprising findings. The parent compound LaOBiS₂ possesses anharmonic ferroelectric soft phonons at the zone center with a rather large polarization of $\approx 10\mu C/cm^2$, which is comparable to the well-known ferroelectric BiFeO₃. Upon electron doping, new unstable phonon branches appear along the entire line $Q = (q, q, 0)$, causing Bi/S atoms to order in a one-dimensional charge density wave (CDW). We find that BiS₂ is a strong electron-phonon coupled superconductor in the vicinity of competing ferroelectric and CDW phases. Our results suggest new directions to tune the balance between these phases and increase T_c in this new class of materials.

PACS numbers: 74.25.Jb, 67.30.hj, 75.30.Fv, 75.25.tz, 74.25.Kc

Superconductivity – a phenomenon first documented in 1911 – remains one of the most challenging subjects of condensed matter physics. Examples of layered superconductors include cuprates[1], MgB₂[2], CaC₆[3], and recent iron-pnictides[4]. Very recently a new family of layered materials, Bi₄O₄S₃[5] and RO_xF_{1-x}BiS₂ (R=La, Nd, Pr, and Ce)[6–9], containing BiS₂ planes was discovered to be superconducting at temperatures up to 10 K. These new systems are structurally similar to the layered, iron-based superconductors LaO_xF_{1-x}FeAs[4], and in both cases the superconductivity is achieved by F-doping. In addition, band structure calculations[11, 12] indicate the presence of strong Fermi surface nesting at the wave vector (π, π) , which is the hallmark property of the Fe-pnictides[4]. These similarities have raised the exciting question of whether or not the superconducting mechanism in the BiS₂ system is related to that in the iron pnictides and have therefore generated enormous interest[5–18].

The fundamental question is whether or not the observed T_c in this new system can be understood within a conventional electron-phonon coupling framework, or is a more exotic mechanism responsible for the superconducting pairing? In this work, we present state-of-the-art first principles calculations that directly address this question and reveal several surprising findings. We show that the parent compound LaOBiS₂ possesses highly anharmonic, ferroelectric, soft phonons at the zone center and a spontaneous polarization of $\sim 10\mu C/cm^2$ that is comparable to that in the well-known multiferroic BiFeO₃. Upon electron doping new instabilities appear along the entire line $Q = (q, q, 0)$, which causes the Bi/S atoms to order into a one-dimensional charge density wave (CDW). We find that BiS₂ is a strong electron-phonon coupled superconductor in close proximity to competing ferroelec-

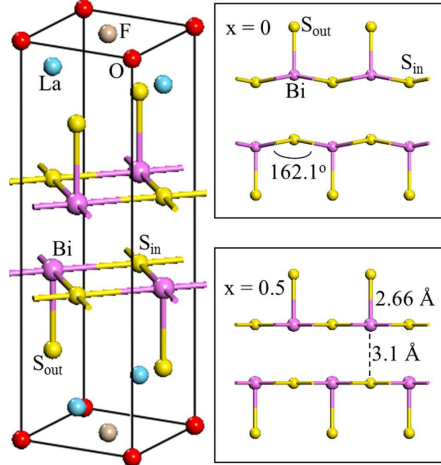


FIG. 1: (color online) Crystal structure of LaO_xF_{1-x}BiS₂ (x=0.5). The side views of the BiS₂ bilayer for x=0 (top) and x=0.5 (bottom) are also shown. Note the zigzag pattern of the BiS₂ plane for x=0.

tric and CDW phases. Our results suggest new directions with which to tune the balance between these phases and increase T_c in this new class of materials.

Figure 1 shows the P4/nmm tetragonal cell of the LaO_xF_{1-x}BiS₂ which consists of two types of atomic layers; namely the LaO spacer and electronically active BiS₂ bilayer. Upon F-doping in the LaO layer, one can control the charge transfer to BiS₂ bilayer and thus tune the electronic properties. In order to simulate such doping in our calculations, we generated 2 × 2 × 1 supercell of LaOBiS₂ and replaced some of the oxygen atoms with F atoms in an ordered fashion with doping levels of x = 0, 0.125, 0.25, 0.375, and 0.5. The results are sum-

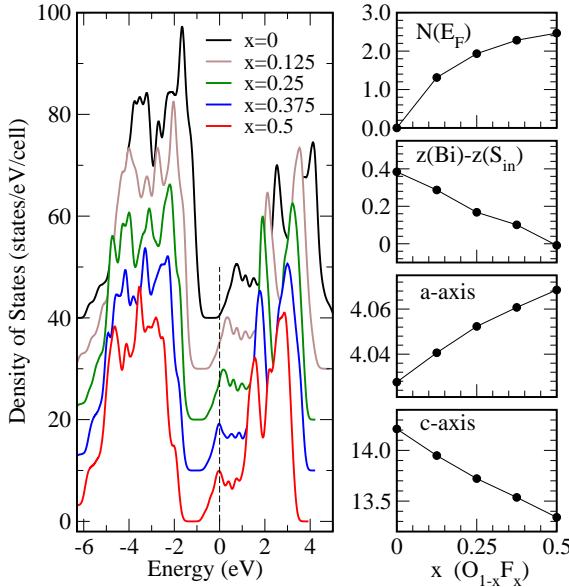


FIG. 2: (color online) Electronic DOS of $\text{LaO}_x\text{F}_{1-x}\text{BiS}_2$ as a function of F-doping x . For clarity the curves are shifted vertically except $x = 0.5$. On the right, $N(E_F)$ (scaled per 10-atom unit cell), lattice parameters and the difference of the z-values (all in Å) of in-plane S (S_{in}) and Bi atoms are also given.

marized in Fig. 2.

The undoped parent compound is a band-insulator with a gap of ≈ 0.8 eV. Upon electron doping, we start to fill the empty states in a rigid-band fashion, turning the insulating parent compound into a metallic system. From the projected density of states (DOS), we determine that the states near the Fermi level are mainly Bi-6p and S-3p character. The density of states at the Fermi level, $N(E_F)$, increases with increasing electron doping and becomes maximal at the half filling $x=0.5$. In agreement with experiments, the c-axis length decreases while the a- and b-axis lengths increase with F-doping. Interestingly the z-values of the in-plane S (i.e., S_{in}) and Bi atoms get closer to each other with doping, yielding a nearly perfect planer structure at $x=0.5$. On the other hand zigzag buckled planes are formed at $x=0$, as shown in Fig. 1. This rearrangement of Bi and S atoms into a perfect planer structure should have important consequences for the electronic band structure and the nature of Fermi surface. Hence it is important to keep an eye on the degree of buckling of BiS_2 plane and its relation to T_c as new isostructural materials are being discovered. We note that similar buckling of CuO_2 plane in cuprates with doping were found to be closely correlated with superconducting temperature[19].

One of the most interesting results shown in Fig. 2 is that $N(E_F)$ is quite high at half-filling ($x=0.5$) and E_F coincides with a peak in the density of states. This usually suggests some sort of instability due to a Van

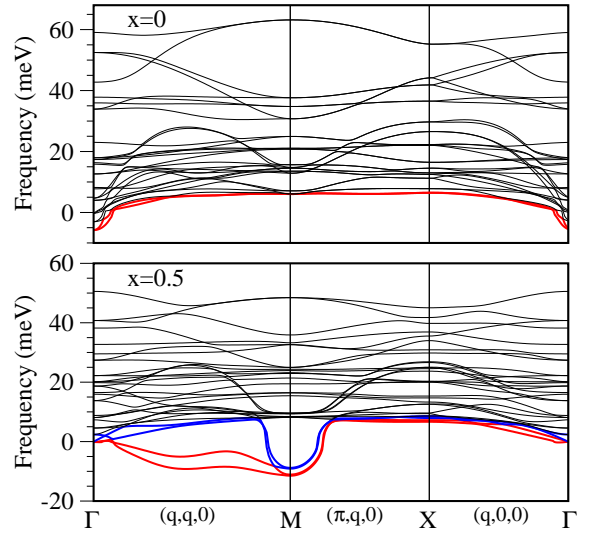


FIG. 3: (color online) Phonon dispersion curves of LaOBiS_2 (top) and $\text{LaO}_0.5\text{F}_0.5\text{BiS}_2$ (bottom), indicating the instabilities at Γ for $x = 0$ and along the entire line $(q, q, 0)$ with the most unstable phonons at M and $(\pi/2, \pi/2)$ for $x = 0.5$.

Hove singularity. In order to check this, we calculated phonon dispersion curves of the parent ($x=0$) and half doped ($x=0.5$) systems using $4 \times 4 \times 1$ supercell and the results are shown in Figure 3. To our surprise, we find that the undoped system shows instability near Γ while the doped system has instabilities along the entire line of $Q=(q,q,0)$ (see also Fig. S2). We repeated the phonon dispersion calculations for $x=0.5$ using a charged system without F-doping and obtained the same instabilities (see Fig. S1), indicating that the soft phonons found here are an intrinsic property of the BiS_2 plane.

In order to have a better insight into the nature of these unstable phonons, we carried out total energy calculations as the system was distorted by the modes having the most negative energy. Figure 4a shows the most unstable soft phonon E_u at Γ for $x=0$, which lowers the symmetry from P4/nmm to P21mn (see Fig. S3). The S atoms move towards Bi atoms along a-axis (or b-axis) and slightly lower the energy of the system by ≈ 1 meV. When the lattice parameters are relaxed, the tetragonal cell becomes orthorhombic and the system energy is further lowered by 0.3 meV. The final structure is shown in Fig. S3. It is remarkable that in the distorted phase, the inversion symmetry is broken and a large spontaneous polarization of $P = 9.9 \mu\text{C}/\text{cm}^2$ is induced despite the rather small displacements. The calculated polarization is comparable to that of the well-known room temperature ferroelectric BiFeO_3 system[20]. However, we note that the potential curve for this unstable ferroelectric phonon mode is quite shallow, as shown in Figure 4, and quantum zero-point motions may not allow such structural distortion. In fact, solving the Schrödinger equation for this potential, we obtained energy levels which

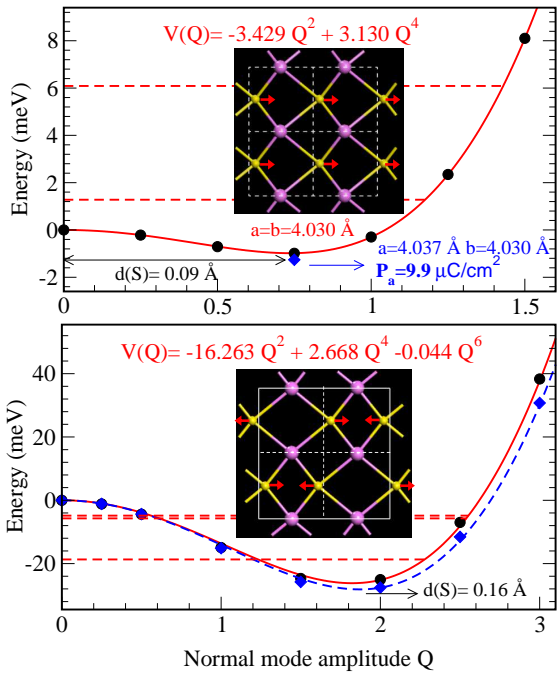


FIG. 4: (color online) Total energy as the system is distorted by the most negative energy phonons in the tetragonal cell of LaOBiS₂ at Γ (top) and in $\sqrt{2} \times \sqrt{2}$ cell of LaO_{0.5}F_{0.5}BiS₂ at $M(\pi, \pi)$ (bottom). The insets show the sketch of the unstable phonons. Horizontal dashed red-lines show the energy levels of the frozen-phonon potential (red curve). The calculated polarization, lattice parameters and the displacement of S atom are also indicated.

are above the potential minimum. Hence, the system should be dynamically disordered due to zero-point motions and should appear as tetragonal. These findings seem to be consistent with the room temperature x-ray data reported so far. Finally, we suggest that the origin of the anharmonic ferroelectric mode could be due to mismatch between the optimum lattice parameters of the LaO and the BiS₂ layers. If the Bi-S bond is forced to elongate due to interaction between LaO and BiS₂ planes, then it is natural for the S atom to break the symmetry and move towards the Bi atom to optimize Bi-S interaction. In fact, repeating the phonon calculations for smaller lattice parameters (i.e. $a=b=3.8$, corresponding to 100 kbar pressure), we do not get negative phonon energies at the zone center any more. Hence, it seems that by changing the spacer oxide, one may tune the nature of the soft phonons and the ground state structure.

Figure 4b shows the total energy in the $\sqrt{2} \times \sqrt{2}$ cell of the tetragonal structure for $x = 0.5$ as it is distorted by the most negative energy phonon mode at (π, π) . Unlike the parent compound, the distortion lowers the system energy significantly, causing S atoms move away by 0.16 Å from the high symmetry site. Solving the Schrodinger equation for the resulting potential curve numerically, we obtained the energy levels which are bound to the

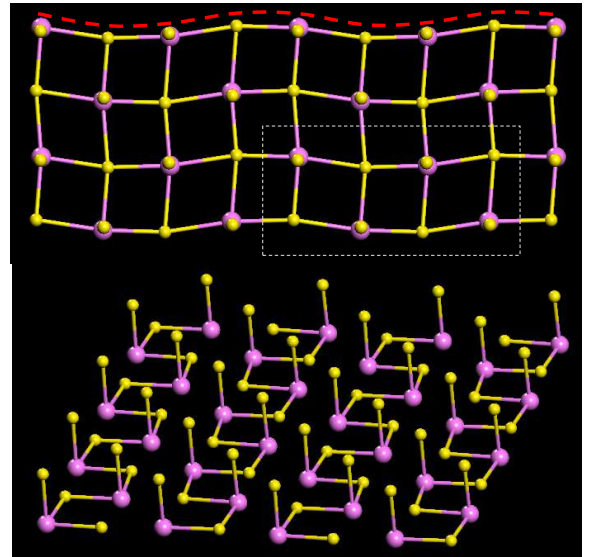


FIG. 5: (color online) 1D Charge Density Wave formation. The BiS₂ plane in fully optimized CDW phase of LaO_{0.5}F_{0.5}BiS₂. Large pink and small yellow spheres are Bi and S, respectively. Dashed red line is to guide the eye, indicating the sinusoidal distortion of the atoms. The white square indicates the $2\sqrt{2} \times \sqrt{2}$ unit cell of the CDW phase. Bottom panel shows the same structure with a Bi-S bond cut-off distance of 2.8 Å. The one dimensional nature of the chains becomes apparent. The intra-chain Bi-S bond is about 2.75 Å while inter-chain Bi-S bond is around 3 Å (see Fig. S3).

local minimum of the distortion. The blue-dashed line in Fig. 4b shows that the same distortion also occurs for the charged system without F-doping. Hence, the observed soft-mode is an intrinsic property of the BiS₂ plane. We next checked whether the (π, π) phonon optimized $\sqrt{2} \times \sqrt{2}$ structure is stable at other q-vectors by repeating the phonon calculations using a $2\sqrt{2} \times 2\sqrt{2}$ super-cell. We obtained more negative energy modes that correspond to the original instability at the $(\pi/2, \pi/2)$ of the $4 \times 4 \times 1$ tetragonal supercell calculations. Hence, we further distorted the $2\sqrt{2} \times 2\sqrt{2}$ structure by the $(\pi/2, \pi/2)$ negative energy phonon and let the system relax. We determined that the optimized structure has the $\sqrt{2} \times 2\sqrt{2}$ unit cell with a rather interesting rearrangement of Bi and S atoms in the BiS₂ plane, as shown in Fig. 5 and Fig. S4. We call this distorted structure as CDW phase, due to the sinusoidal distortion of the Bi and S atoms as shown by red dashed lines in Figure 5. Unlike the $x = 0$ case, applying pressure or using smaller lattice constants in the phonon calculations does not stabilize the negative energy phonons. Hence, it is tempting to conclude that the origin of this distortion is due to strong Fermi surface nesting at M[11, 12]. However, we note that the soft phonon branch occurs along the entire line $Q = (q, q, 0)$ and not just at the M point. Hence, in addition to Fermi surface nesting, there should be an important structural reason as well for the observed soft

modes. Finally, by looking at the bond distances between Bi-S, we notice that there are one-dimensional channels of Bi-S bonding as shown in Fig. 5. Interestingly, from Hall Effect measurements¹⁴ it was concluded that superconducting pairing occurs in one-dimensional chains in these systems, which could be related to the CDW phase predicted here. Similarly, high pressure measurements reveal non-monotonic dependence of T_c on pressure and suggest that the Fermi surface of $\text{LaO}_x\text{F}_{1-x}\text{BiS}_2$ could be in the vicinity of instabilities[10]. Finally, the x-ray powder diffraction[6] for $\text{LaO}_{0.5}\text{F}_{0.5}\text{BiS}_2$ shows rather unusual broad peaks, which could be again related to the CDW phase.

We next address the nature of superconductivity found in these BiS_2 layered systems. We carried out el-ph coupling calculations using both (π, π) phonon optimized $\sqrt{2} \times \sqrt{2}$ and CDW structures. We consider $2\sqrt{2} \times 2\sqrt{2}$ supercells, containing 80 atoms and obtain the el-ph coupling by the frozen-phonon method. The results are summarized in Figure 6. In both (π, π) -optimized or fully distorted CDW structures, the Eliashberg functions are quite similar, indicating that the main physics of the electron-phonon coupling mechanism does not depend on the details of the structure. In the (π, π) -phonon optimized structure, $N(E_F)$ is higher than in the CDW phase, and therefore leads to higher el-ph coupling. The total electron-phonon coupling is $\lambda = 0.83$ with a logarithmic frequency average $\omega_{log} = 101 \text{ K}$. These values give a maximum superconducting temperature of $T_c = 8.5 \text{ K}$. Even in the fully distorted CDW phase, we get quite large electron-phonon coupling $\lambda = 0.6$ and a logarithmic frequency average $\omega_{log} = 122 \text{ K}$, which gives a T_c of 6 K. These values are in excellent agreement with the reported experimental values of T_c which vary from 3K to 10 K, depending on the level of doping and sample quality. Inspecting the modes which give the highest el-ph coupling, we estimate that about 90% of λ comes from in-plane Bi and S phonons while the remaining 10% is due to phonons along the c-axis. There are two bands of phonons near (5 to 10) meV and (15 to 25) meV. The phonons in the lower energy band are due to coupled Bi and S motion while the phonons in the high energy bands are due to almost pure S oscillations. Animation of these modes can be found in Ref.24. In Figure 6, we also show the total phonon density of states along with the atomic-projections of the DOS. As expected based on the masses of atoms, O and F-based phonons are above 30 meV and do not produce much el-ph coupling. The La phonons are near 10 meV but, as expected, do not produce any significant el-ph coupling.

In conclusion, we have discovered rather unusual structural and dynamical properties of LaOBiS_2 with electron doping. The large-amplitude in-plane S-atom displacement controls the structural properties and gives rise to large el-ph coupling. It would be interesting to measure the isotope effect for the S atom, which may be uncon-

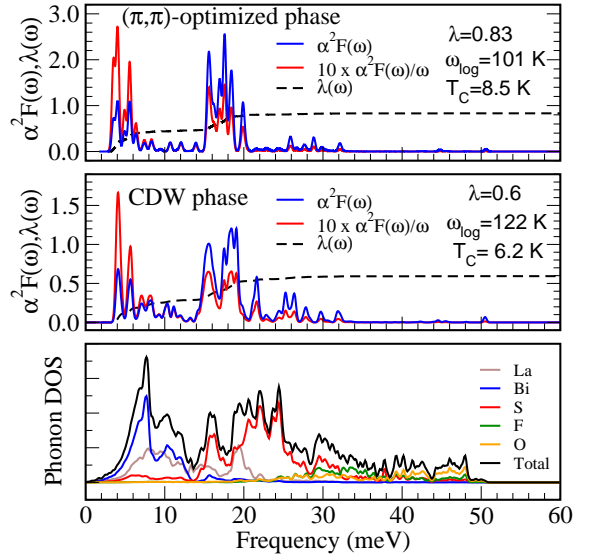


FIG. 6: (color online) Eliashberg functions in partially optimized (top) and fully optimized CDW structure (middle). El-ph coupling constant λ , T_c , ω_{log} are also given. The total and atomic-projected phonon DOS are shown in the bottom panel.

ventional. Our results also suggest that thin films of BiS_2 on various substrates may exhibit unusual properties due to epitaxial strain at the interface. New materials with similar structures but with BiO_2 plane could be quite interesting due to smaller mass of oxygen atom, which gives higher phonon energies, and in turn higher T_c . In fact, the results reported here remind us of another interesting system, namely $\text{Ba}_{1-x}\text{K}_x\text{BiO}_3$ [25], which exhibits several complicated structural phases[26] and superconductivity at 31 K[25]. It is too early to say which of these predictions from DFT calculations will be demonstrated experimentally. However it is clear that the BiS_2 based layered systems are very rich in physics, involving nearly ferroelectric soft phonons and CDW ordering along with strongly coupled electron-phonon superconductivity.

Acknowledgments: We acknowledge many fruitful discussions with A. B. Harris and P. M. Gehring. TY acknowledges partial support by the U. S. Department of Energy through BES Grant No. DE-FG02-08ER46522 for the computational resources used in this study.

Supporting Information: The details of methods and additional plots of the phonon dispersion curves, picture of optimized structures and atomic positions/lattice parameters are given in supporting information (SI).

* Electronic address: taner@seas.upenn.edu

- [1] Orenstein, J. and Millis, A. J. Science **288**, 468 (2000).
- [2] Nagamatsu, J., Nakagawa, N., Muranaka, T., Zenitani, Y. and Akimitsu, J. Nature **410**, 63 (2001).

- [3] Weller, T. *et al.* Nature Phys. **1**, 39-41 (2005).
- [4] Takahashi, H., Igawa, K., Arii, K., Kamihara, Y., Hirano, M., Hosono, H. Nature, **453**, **376**, (2008).
- [5] Mizuguchi, Y., *et al.*, arXiv:1207.3145 (2012).
- [6] Mizuguchi, Y., *et al.*, arXiv:1207.3558 (2012).
- [7] Demura, S., *et al.*, arXiv:1207.5248 (2012).
- [8] Jha, R. *et al.*, arXiv:1208.5873 (2012).
- [9] Xing, J. *et al.*, arXiv:1208.5000 (2012).
- [10] Kotegawa, H., *et al.*, arXiv:1207.6953 (2012).
- [11] Usui, H., *et al.*, arXiv:1207.3888v1 (2012).
- [12] Wan, X., *et al.*, arXiv:1208.1807v1 (2012).
- [13] Zhou, T. and Wang, Z. D. arXiv:1208.1101v1 (2012).
- [14] Li, S., *et al.* arXiv:1207.4955v1 (2012).
- [15] Awana, V. P. S., *et al.*, arXiv:1207.6845 (2012).
- [16] Takatsu, H. *et al.*, arXiv:1208.2796 (2012).
- [17] Sathish, C. I. and Yamaura, K., arXiv:1208.2818 (2012).
- [18] Lei, H. *et al.*, arXiv: 1208.3189 (2012).
- [19] Chmaissem, O. *et al.*, Nature **397**, 45 (1999).
- [20] Ederer, C. and Spaldin, N. A. Phys. Rev. Lett. **95**, 257601 (2005).
- [21] Giannozzi, P. *et al.* J. Phys. Condens. Matter **21**, 395502 (2007).
- [22] Blochl P. E. Phys. Rev. B, **50**, 17953 9 (1994).
- [23] Lam, P. K., Dacorogna, M., Cohen, M. L. Phys. Rev. B **34**, 5065 (1986).
- [24] Animations of the phonons that give the largest el-ph coupling in $\text{LaO}_x\text{F}_1 - x\text{Bi}_2\text{S}_3$ can be found at <http://www.nenr.nist.gov/staff/taner/bis2superconductors>
- [25] Cava, R. J. *et al.* , Nature **332**, 814 (1988).
- [26] Braden, M *et al.*, Rev. B **62**, 6708 (2000).

SUPPORTING INFOMATION

1. Methods The first-principles calculations were performed within the plane-wave implementation of the Perdew-Burke-Ernzerhof generalized gradient approximation to density functional theory as implemented in the PWSCF package[21]. We used Vanderbilt-type ultrasoft potentials. The wavefunction and charge cutoffs are taken as 40 Ry and 480 Ry, respectively. We tested that k-sampling converges well with a k-point grid of 20x20x6 in the tetragonal cell. For $\sqrt{2} \times \sqrt{2}$ structure, we used k-mesh of 14x14x6. The structures are optimized until the forces on atoms are less than 0.005 eV/Å and the stress is less than 0.01 kbar. Some of the total energy and phonon calculations were also repeated by Vienna Ab-Initio Simulation Package using more accurate Projector Augmented Waves method[22]. We obtained very similar results concerning the structural distortion, soft phonons and their energies. Finally, the electric polarization is calculated by PWSCF via the modern theory of polarization (i.e. Berry Phase). We used 20x20x6 k-grid for self-consistent calculations and the polarization is calculated using twice dense k-grid along the calculated polarization direction. The phonon dispersion curves were obtained by the direct finite displacement method. We used 0.02 Å displacements in plus and minus directions to obtain the force-constant matrix numerically. Once we

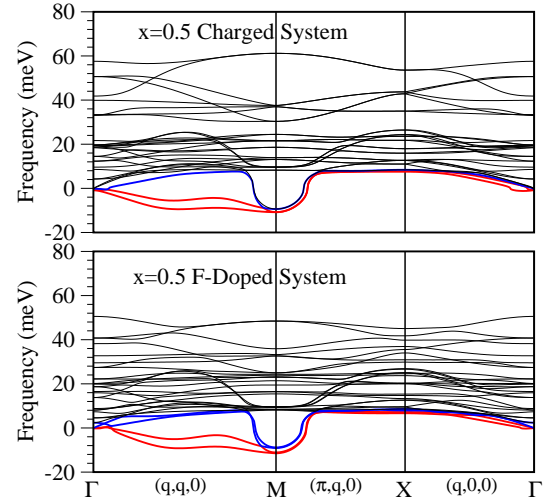


FIG. S1: Phonon dispersion curves for $x=0.5$ with charged system without F-doping (top) and with F-doped case (bottom).

have the phonon spectrum, the electron-phonon coupling is calculated by the supercell frozen-phonon method[23]. Briefly, for a given phonon branch, the system is distorted according to the normal mode by its root-mean-square (rms) value and then the electron-phonon matrix element, $M_{n,n'} = \langle n | H_p - H_0 | n' \rangle$, is calculated self-consistently using the wave-functions ($|n\rangle$) and eigenvalues (E_n) of the total potential H_p , H_0 (i.e., frozen-phonon and reference cell, respectively). The el-ph coupling constant λ is then obtained from the Fermi surface averaging of $M_{n,n'}$ using gaussian smearing method. The superconducting critical temperature T_c , was estimated using the Allen-Dynes formula, with $\mu^* = 0$ for the upper limit of T_c .

2. Phonon Dispersion Curves in the Electron-Doped System without F-substitution

Here we compare the phonon dispersion curves obtained from $4 \times 4 \times 1$ supercell of the tetragonal LaOBiS_2 cell with $x = 0.5$ doping level (top panel in Fig. S1) with the one obtained from actual F-substituted system (bottom panel in Fig.S1). Note that both systems show the same phonon instability along the entire line $Q = (q, q, 0)$. Hence the predicted soft modes do not depend on the details of the doping and it is intrinsic to the Bi_2S_3 plane. The main difference between the actual F-doping and just adding an electron to the system is the maximum phonon energies. In the case of charge doping, the top phonon bands extend up to 60 meV (which is similar to undoped case). The upper phonon band is somewhat separated from the bottom phonon bands. In the case of F-doping, the top-phonon band gets softer and mixed up with the lower energy phonon bands. This is expected as the F-atom has smaller diameter than oxygen atom and when F is substituted at the oxygen site, there will be more room for the surrounding atoms to

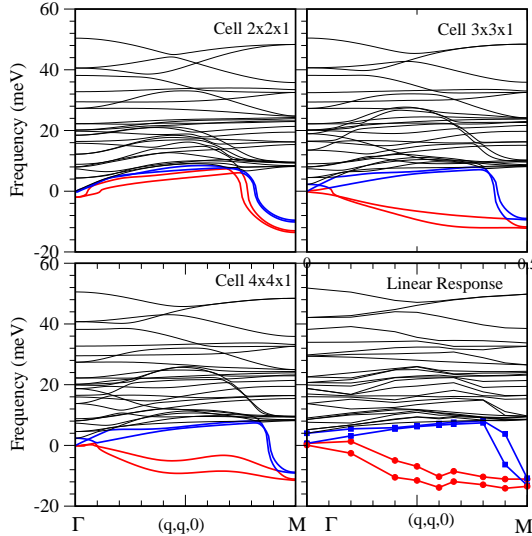


FIG. S2: Phonon dispersion curves from different supercells and the linear response theory, all showing that we have two unstable phonon branches along the entire line $(q,q,0)$.

oscillate easily, thus yielding lower phonon energies.

3. The soft-phonon branches along the entire $(q,q,0)$ direction for $\text{LaO}_x\text{F}_{1-x}\text{BiS}_2$

In Fig. S2 we present the phonon dispersion curves along $(q,q,0)$ direction which is obtained from different supercells, namely $2 \times 2 \times 1$, $3 \times 3 \times 1$, and $4 \times 4 \times 1$ of the $\text{LaO}_x\text{F}_{1-x}\text{BiS}_2$. We also calculated the same dispersion curve using the linear response theory, which does not assume any supercell. We note that in $2 \times 2 \times 1$ supercell, the calculations have the exact phonon energies only at $(0,0,0)$ and $(\pi,\pi,0)$ and therefore does not reflect the correct dispersion curve. For $3 \times 3 \times 1$ supercell, we have exact phonon energies at $Q = (n2\pi/3, m2\pi/3, 0)$ ($n, m = 0, 1, 2$). For $4 \times 4 \times 1$ supercell, the exact phonon energies are at $Q = (n2\pi/4, m2\pi/4)$ ($n, m = 0, 1, 2, 3$). In supercell calculations the smooth dispersion curves are obtained by assuming a real-space cutoff distance for the force-constant matrix. From Figure S2, it is clear that we need at least $3 \times 3 \times 1$ supercell to get the right dispersion curves. The linear response theory, in excellent agreement with the supercell calculations, also shows that there are two unstable phonon branches along the entire $Q = (q,q,0)$ direction. In Figure S3, we show only the raw-data from linear response theory calculations, without making any approximation for the real-space force constants and cutoff, that is needed to get the smooth curves.

4. The Ferroelectric Phase of LaOBiS_2

Figure S3 shows the structural parameters of the fer-

roelectric phase of LaOBiS_2 after the tetragonal structure is distorted by the most negative energy mode and then fully relaxed. The lattice parameter along the S-displacement direction gets longer, causing one-

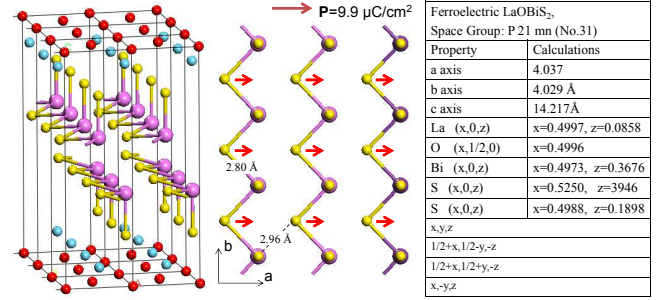


FIG. S3: The ferroelectric phase of LaOBiS_2 which is obtained by first distorting the tetragonal phase using the most unstable gamma-phonon and then by performing full structural relaxation. The bond-stick model shows only the bonds with bond-distance of 2.8 \AA to emphasize the one-dimensional chain perpendicular to the in-plane S-displacements (shown by red arrows). The Table on the right shows the optimized structural parameters as well as the symmetry operations of the ferroelectric phase.

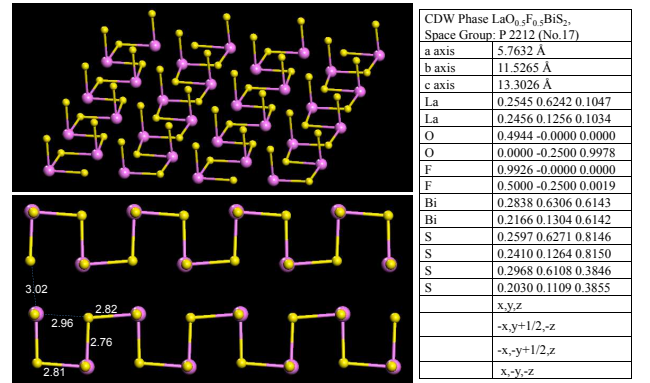


FIG. S4: The CDW phase of $\text{LaO}_{0.5}\text{F}_{0.5}\text{BiS}_2$ with the one-dimensional chains. Various Bi-S distances are also shown. On the right, we give the structural parameters and the symmetry operators of the CDW phase.

dimensional Bi-S zigzag chains perpendicular to the S-displacement with intra-chain Bi-S bond distance of 2.8 \AA and inter-chain Bi-S bond distance of 2.96 \AA .

5. The CDW Phase of $\text{LaO}_{0.5}\text{F}_{0.5}\text{BiS}_2$

Figure S4 shows the structural parameters of the CDW phase of $\text{LaO}_{0.5}\text{F}_{0.5}\text{BiS}_2$ after the tetragonal structure is distorted by the most negative energy modes at (π,π) and $(\pi/2,\pi/2)$, respectively, and then fully relaxed.